

# Computational modelling of the micromechanics of void growth and coalescence in ductile failure via the Discrete Element Method

Rubén Galiano Batista, Ignacio Iturrioz

*PROMEC, Universidade Federal do Rio Grande do Sul, Porto Alegre, RS – Brazil*

Adrián P. Cisilino

*División Soldadura y Fractomecánica – INTEMA, Facultad de Ingeniería,  
Universidad Nacional de Mar del Plata, Mar del Plata – Argentina*

## Abstract

The micromechanics of ductile failure due to void growth and coalescence in a micro-porous metal-matrix material are studied in this paper by using the Discrete Element Method (DEM). The DEM was selected for the numerical analyses due its inherent ability to handle crack nucleation and void coalescence. The study is carried out using a series of representative volume elements (RVE) of the pseudo-microstructure of a ferritic nodular cast iron. The DEM models are used to correlate the stress vs strain behaviour of the RVEs with the evolution of the strain and damage energy and the void volume fraction. Special attention is given to the occurrence of void coalescence and final failure. Computed void volume fractions are in good agreement with other visited reports. Obtained results demonstrate the effectiveness of the DEM to provide further understanding of the micro-mechanics of failure in nodular cast iron.

Keywords: micro-porous metal-matrix material, discrete element method, damage mechanics

## 1 Introduction

The ductile failure of metallic materials most often occurs by nucleation, growth and coalescence of microvoids. For most of the engineering alloys, voids can be nucleated from non metallic inclusion and second phase particles by particle fracture or interface decohesion. One of the best known micromechanical models in this area is due to Gurson [1], which uses the volume fraction,  $f$ , as the main parameter to characterize the material damage.

In materials where there is a strong interaction between the particle and metallic matrix, the nucleation stage is the dominant one in the failure process. On the other hand, when there is weak particle – metallic interaction, the dominant stage is void coalescence [2]. The present work focuses on the later case.

Direct experimental observation of the evolution of the micromechanics of void nucleation, growth and coalescence is very difficult task due to the problem length-scale. As a consequence, there are very few works dedicated to the in situ observation of the micromechanics of the failure process. One of them is the work [3], which is main reference for this work.

Computational mechanics has shown itself as an efficient tool to help understanding the void growth and coalescence phenomena. Thus, an extensive number of works have been carried out in order to study the influence of mechanical and metallurgical parameters such as the initial void volume fraction  $f_0$ , shape and size of voids, stress triaxiality, etc., on the behavior of void growth and coalescence. [4]. Most of this works have been carried out via Finite Element Analyses (FEA) on unit cells models, i.e. considering a microstructure with a periodic distribution of voids.

It is proposed in this work to study the micromechanics of void growth and coalescence considering the actual (non-regular) distribution of voids for a metal-matrix material. This is done using DEM models and considering a Ferritic Nodular Cast Iron (FNCI) as model material. The study is carried out using a series of representative volume elements (RVE) of the material microstructure. Computations are used to correlate the stress vs strain behaviour of the RVEs with the evolution of the strain and damage energy and the void volume fraction. Obtained results demonstrate the effectiveness of the DEM to provide further understanding of the micro-mechanics of failure in nodular cast iron.

Due to space limitation no details about the formulation of the DEM are given in this work. The reader can found the details of the DEM implementation in other work presented in this Conference (see [5]).

## 2 Topological characterization of the material microstructure

The reference material consists in a Ferritic Nodular Cast Iron (FNCI) with an initial void volume fraction  $f_0 = 0,077$ . The distribution of the graphite nodules in the microstructure was characterized via a statistical analysis of a series of micrographs (Fig. 1a), with nodular counts in the range from 60 to 600 nodules per  $\text{mm}^2$ . In every case nodules were considered perfectly circular. The topology of the nodule distribution was characterized using the following parameters: the nodule radii ( $r$ ), the distance to the nearest neighbor ( $d$ ), the number of nearest neighbors ( $N$ ), and the mean distance to the nearest neighbors (see Fig. 1(b)). Geometrical data was retrieved from the micrographs using image analysis software, and then processed using a Delaunay triangularization algorithm in order to compute the number of neighbors and the correspondent distances. The process is illustrated in Fig.1(b,c and d).

The results from the statistical study showed that the distribution of nodules is almost independent on the nodular count when the ratio  $d/r$  is chosen as a parameter. Based on this conclusion, and bearing in mind that the 3D volume fraction of spherical inclusions of a representative volume element coincides with the 2D volume fraction (area fraction) of its cross section [6], the nodule radius  $r$  was chosen as the characteristic length for the generation of the geometries of the DEM models. Thus, the model geometries consisted in random distributions of non-overlapping nodules of identical size, Fig.1(d). This geometry possesses mean values for  $(d/r)_{cl} = 3.91$ ,  $(d/r)_{nat} = 6.99$  and  $N = 5.96$ , which are well in accordance with those computed from the micrographs. This correspondence was verified

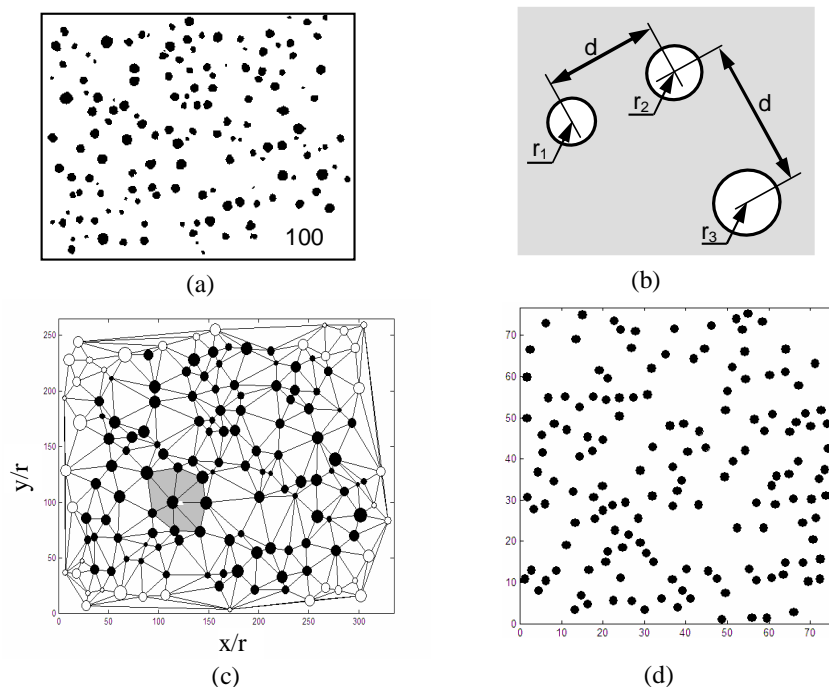


Figure 1: (a) Micrograph of the nodular cast iron microstructure; (b) Geometrical parameters used in the geometrical characterization of the microstructure; (c) Delaunay triangularization of the positions of the nodules for the micrograph shown in (a); and (d) Example of a randomly generated microstructure containing 150 nodules.

for the computer generated models in all the range of node counts  $N_{area}$ . The mechanical properties of the material are given in Table 1 (from [3]).

Table 1: Mechanical properties of reference material (Berdin 2001)

E (MPa)	$\sigma_u$ (MPa)	$\sigma_y$ (MPa)	Elongation %	$K_{IC}$ (MPa·m <sup>1/2</sup> )	$f_0$ %
187000	390	260	23	77	7,7

### 3 Void volume fraction computation

Damage characterization presented by [3] showed that the interface between the graphite nodules and the metal matrix in the ferritic cast iron is very weak, and then the material behaves essentially as a porous material with the graphite nodules acting as voids in an elastic-plastic matrix. This behaviour was introduced in the numerical models by setting a reduced value of the specific fracture energy to the elements coincident with the location of the nodules (see Figure 2). Since the weakened elements result with a very low load-carrying capacity, and thus their mechanical behaviour can be assimilated to that of voids.

Using the same criteria, the evolution of void volume fraction with the applied load was monitored by computing the actual number of elements which have lost their load-carrying capacity (weakened and failed elements). This is done by adding the individual contributions of each DEM module. In this way, the volume fraction for the  $i^{th}$  module is computed as the quotient between the number of weakened,  $n_{weakened}^i$ , and failed,  $n_{failed}^i$ , elements and the total number of elements of the module,  $n_{total}^i$  ( $n_{total}^i = 26$  for the cubic module used in this work)

$$f = \frac{\sum_{i=1}^m V_i \cdot \frac{n_{weakened}^i}{n_{total}^i} + \sum_{i=1}^m V_i \cdot \frac{n_{failed}^i}{n_{total}^i}}{\sum_{i=1}^m V_i} \quad (1)$$

where  $V_i$  represents module volume.

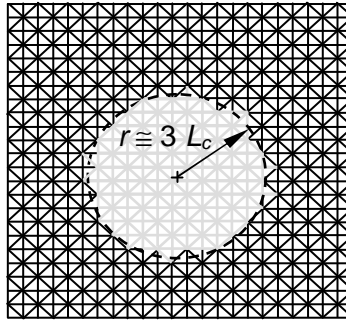


Figure 2: Procedure for the introduction of initial voids into the DEM model (Note that only those elements with their centroids located within the nodule domain are selected and weakened).

The result of a convergence analysis showed that three DEM modules in the direction of the nodule radius are necessary in order to represent initial void volume fraction,  $f_0$ , with an error less than 0,15%.

#### 4 Determination of the representative volume element size

The Representative Volume Element (RVE) is the smallest material volume that presents a macroscopic invariant response. The material sample must be big enough to contain a high number of heterogeneities (graphite nodules in this case) and to present and to possess small boundary field fluctuations relative to its size [7].

In order to size the RVE, a series of DEM analysis were performed for samples containing an increasing number of nodules. Consistently with the Hill's condition [8] the samples were subjected to biaxial traction boundary conditions. The following nodule per sample sequence was considered: 2, 5, 10, 20, 40, 60, 70 and 80. Ten different configurations were tested for each sample size.

In every case the following information was monitored: the elastic strain energy density,  $u_{el}=U_{el}/V$ , the damage energy density  $u_{damage}=U_{damage}/V$ , and the void volume fraction  $f$ . These control parameters were computed at characteristic points of the stress vs strain curve:  $P_1$ : linear elastic regime;  $P_2$ : non linear regime; and  $P_3$ : maximum stress, (Fig. 3(a)). Obtained results are shown in Figures 3 and 4 in terms of the mean values resulting from the ten analyzed geometries for each sample size considered. The dispersion of the results is represented by means of the error bars.

It is found that the elastic strain energy results present a nice behaviour in the linear and non-linear regimes. Dispersion of the results for 30 nodules is less than 0.5% in the linear regime (Figures 3b) and around 8% for the non-linear regime (Figures 3c). On the other hand, the dispersion is close to 30% at maximum load (Figure 3d). Damage energy results for the non-linear regime and at maximum load (Figures 4a and 4b) behave similarly to their elastic energy counterparts.

Results for the void volume fraction are presented in Figure 4(c). Results in the linear and non-linear regimes are independent of the sample size for models containing more than 20 nodules. Dispersions of the results for these cases are less than 0.2%. Once again, results for the maximum load present dispersions around 30%.

From the analysis of the above results, it is found that accurate computations with dispersions of only a few percent could be obtained in the linear and non-linear regimes using models containing 40 nodules (voids). On the other hand, results computed at maximum load exhibit dispersions around 30%, even when the size of the samples is enlarged to contain up to 80 nodules. However, it is worth noting that although these dispersions mean values do not present important variations with the sample size. Based on these conclusions models containing 40 nodules were selected as RVE for the following analyses.

#### 5 Application to tension test

Forty RVEs DEM models containing 40 nodules each were subjected to uniaxial traction in order to study the evolution of the damage in the pseudo-micro-structure. Fig. 5 illustrates the mean value and standard deviation (y-error bars) of the resulting stress vs strain curve together with the actual behaviour of one sample reference material [3]. It can be observed that the numerical and experimental results are in excellent agreement up to the point where the maximum load is attained in the numerical models ( $\varepsilon_{22} \approx 0, 12$ ) and then start diverging. However, experimental data are always contained within

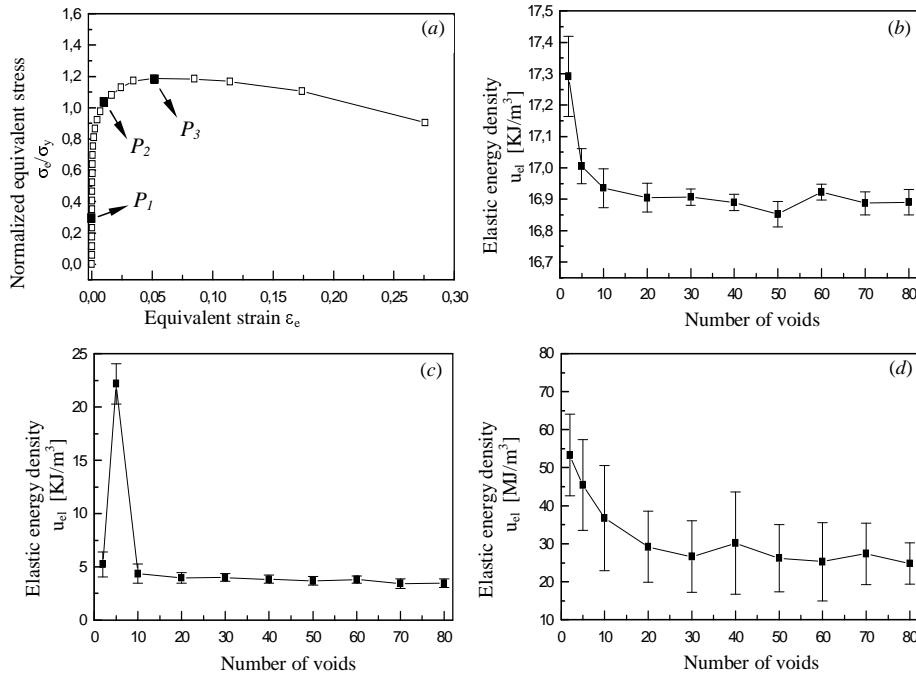


Figure 3: Determination of the RVE size: (a) identification of the control points on the stress-strain curve. Results for the elastic strain energy density  $u_{el}$ .: (b) the linear regime ( $P_1$ ), (c) The non linear regime ( $P_2$ ), and (d) the maximum stress ( $P_3$ ).

the standard deviation of the numerical results.

The evolution of the damage in the microstructure is depicted using a series of subfigures in Fig. 5. Black areas in the subfigures correspond to damaged elements. Subfigure (a) shows the localization of the damage in the ligaments between the nodules in the early stages of the non-linear portion of the stress vs strain curve. Damage localization progresses with the increment of the load up the point where coalescence starts (see circled detail in Subfigure b). Finally, subfigure (c) illustrates the stage of advanced damage, with void growth and coalescence extensively spread over the specimen domain.

The following sections are devoted to discuss the two characteristic phenomena of the micromechanics of failure: void coalescence and final failure.

### 5.1 Void coalescence

Coalescence is considered to occur in this work when the complete failure of the ligament between the voids takes place. This criterion aims to quantify the actual void fraction at the onset of coalescence ( $f_c$ ). Note that this criterion differs from that proposed by other authors which for elastic-perfectly

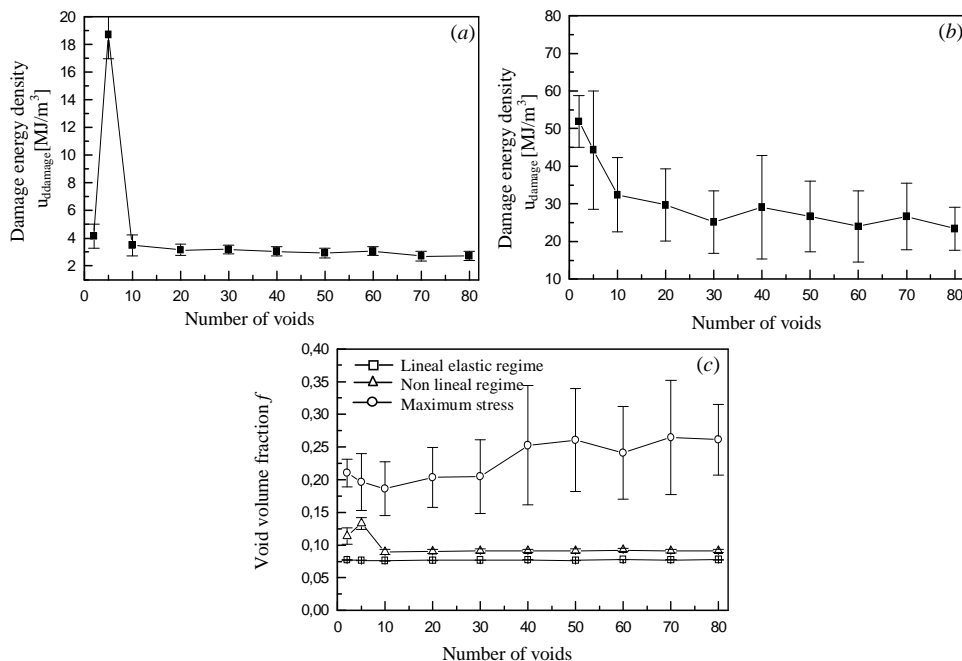


Figure 4: Results in terms of damage energy density  $u_{damage}$  and fraction void volume  $f$  for the samples with different number of nodules. (a)  $u_{damage}$  in the non linear control point,  $P_2$ ; (b)  $u_{damage}$  in the maximum stress control point,  $P_3$ . (c)  $f$  in the three control points. Error bars indicates the dispersion in the results.

plastic materials associate coalescence to the plastification of the ligament between nodules [4, 9, 10].

The strain at the onset of coalescence for all the forty RVE models is shown in Figure 6 (a). The average macroscopic strain value for the onset of coalescence is  $\varepsilon_{22}^c = 0.12$ , with a standard deviation  $\Delta = \pm 0.035$  (see shaded band in Figure 6). Note that the average strain value for coalescence,  $\varepsilon_{22}^c$ , corresponds to the maximum load attained by the numerical models (point “b” in Fig. 5).

Fig.6 (b) illustrates mean evolution of the void volume fraction in terms of the longitudinal strain  $\varepsilon_{22}$ , with y-error bars indicating the dispersion of the results. The strain range corresponding to the onset of coalescence (Fig.6), was used to estimate the critical void volume fraction  $f_c$ . The resulting mean value for the critical void volume fraction is  $f_c = 0.19$ , with lower and upper bounds  $f_c^{\min} = 0.12$  and  $f_c^{\max} = 0.27$ , respectively. This range exhibits a reasonable agreement with the standard values reported in the literature, which are in the range from  $f_c = 0.10$  to  $f_c = 0.20$  [4, 9, 10]. The maximum discrepancy is found for the upper bound, where as shown in Section 4, the void volume fraction results of the DEM present the maximum dispersion.

The void volume fraction at the onset of coalescence reported for the reference material is  $f_c =$

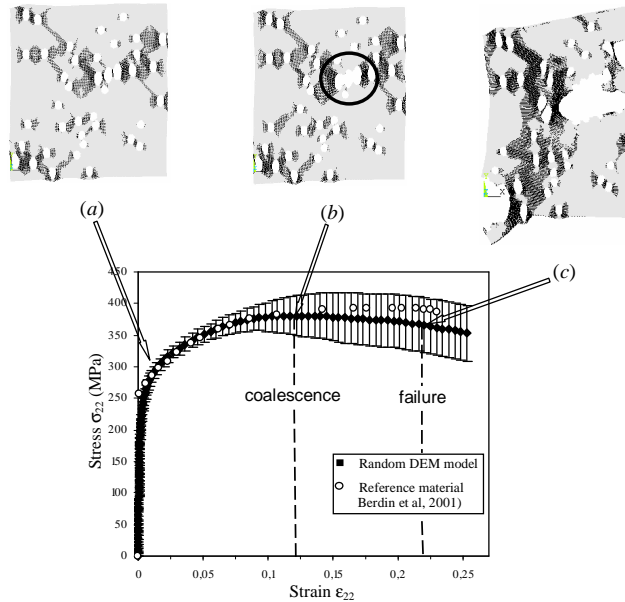


Figure 5: Mean value and standard deviation (y-error bars) of the uniaxial stress vs strain curve resulting from DEM analyses for the forty RVEs. Subfigures illustrate the evolution of the damage with the applied load.

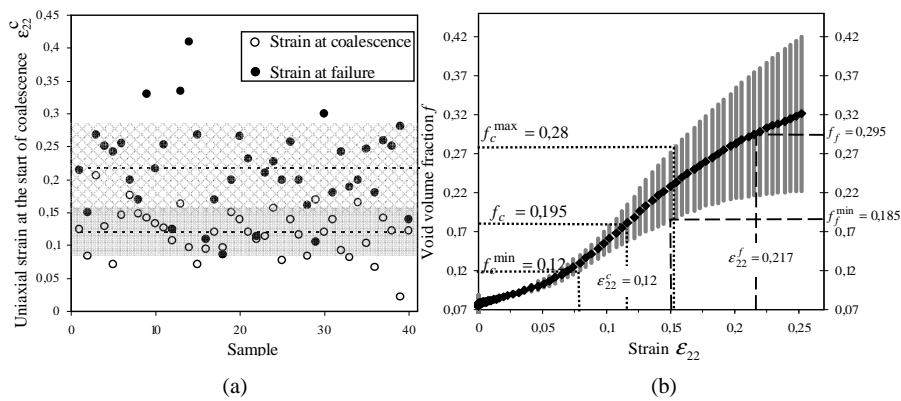


Figure 6: Void coalescence and failure results: a) Uniaxial strain values corresponding to the onset of void coalescence and final failure for the forty EVRs (The dashed line and the shaded band indicate mean value and standard deviation of the results, respectively); b) Evolution of the void volume fraction as a function of the longitudinal strain

0.12 [3]. This value results lower than the mean  $f_c = 0.19$  computed in this work and a number of reasons could help explaining this discrepancy. The first consideration is related to the concept of coalescence itself. As stated earlier in this section, coalescence is considered to occur in the DEM models when two voids (nodules) merge, while as mentioned earlier, the usual criteria in the literature associates coalescence to flow localization in the ligament between voids. Thus, it could be expected that the DEM models will detect coalescence “later” during the loading process. At the same time it is worth to note that the value of  $f_c$  reported by [3] does not correspond to actual experimental observations, but it was calibrated in order to adjust a Gurson model to the test data. Another important issue to consider when comparing the DEM results to that of [3] is stress triaxiality. It is well known that Gurson model assumes a high level of stress triaxiality and the dependence of  $f_c$  on stress triaxiality is pronounced. Kim et al [4] report increments of up to 80% in  $f_c$  when reducing the stress triaxiality for a material containing an initial volume fraction  $f_o = 0.05$ . They also show that this tendency can further increase when augmenting the initial volume fraction. Thus, if it is considered that computations in this work are performed for RVEs subjected to low triaxiality levels (two-dimensional plane-stress models) with an initial void volume fraction  $f_o = 0.077$ , relatively high levels of the critical void volume fraction could be expected.

## 5.2 Final failure

The final failure was monitored for the forty RVE and the results in terms of the macroscopic uniaxial strain are presented in Fig. 6 (a). The mean value for the failure strain is  $\varepsilon_{22}^f = 0.217$  with a standard deviation of  $\Delta = \pm 0.067$ . The computed mean failure strain value is close agreement with the result reported by Berdin et al (2001) (see Table 1).

The strain range for failure was used to estimate the void volume fraction at failure  $f_f$  (see Fig. 6 (b)). The resulting mean value is  $f_f = 0.295$ , with lower and upper bounds  $f_f^{\min} = 0.185$  and  $f_f^{\max} = 0.42$ , respectively. When compared to the results reported by [3] and [11] for the reference material,  $f_f = 0.20$ , it is found that the computed values are almost coincident with the computed lower bound. As argued for the coalescence results in the previous section, the relatively large dispersion encountered for the void volume fraction results at failure can be partially attributed to the size of the RVE.

## 6 Conclusions

A Discrete Element Method (DEM) formulation for the analysis of the micro-mechanics of failure by grow and coalescence of voids was presented in this paper. The DEM was selected for the numerical analyses due its inherent ability to handle crack nucleation and void coalescence. The microstructure of the cast iron was assimilated to that of porous materials, with the graphite nodules acting as voids in an elastic-plastic matrix. The topology of the microstructure was characterized from the statistical analysis of measurements performed on standard micrographs using image-processing. DEM models were carried out using two-dimensional computer-generated microstructures which reproduce the distribution of nodules of the material.

The size of the Representative Volume Element (RVE) was determined using a series of DEM

models performed for samples containing an increasing number of nodules. The strain energy density, the damage energy density, and the void volume fraction were monitored throughout the tests till an invariant macroscopic response was found for the linear and non-linear regimes. Finally, a RVE containing 40 nodules was selected.

The extension for a 3D analysis is possible; the great limitation, in this case, is the computational cost.

The proposed methodology demonstrates the effectiveness of the DEM to provide further understanding of the micro-mechanics of failure by grow and coalescence of voids. The developed tool could be easily adapted to include the effect of inclusions, inhomogeneities in the matrix mechanical properties.

### Acknowledgements

This work was partially supported by grants CAPES/SECYT BR/PA02-EXII/007 (Fundação Coordenação de Aperfeiçoamento de Pessoal Nível Superior, Brazil and Secretaría de Ciencia Tecnología e Innovación Productiva, Argentina), PROSUL 040/2006 (Conselho Nacional de Desenvolvimento Científico e Tecnológico, Brazil) and PICT 12-12528 (Agencia de Promoción Científica y Tecnológica de la República Argentina).

### References

- [1] Gurson, A., Continuum theory of ductile rupture by void nucleation and growth: Part i- yield criteria and flow rules for porous ductile media. *Journal of Engineering Materials and Technology*, **99**, pp. 2–15, 1977.
- [2] Anderson, T., *Fracture Mechanics: Fundamentals and Applications*. Master's thesis, Department of Mechanical Engineering - Texas A&M University, College Station - Texas, 1991.
- [3] Berdin, C., Dong, M. & Prioul, C., Local approach of damage and fracture toughness for nodular cast iron. *Engineering Fracture Mechanics*, **68**, pp. 1107–1117, 2001.
- [4] X., K.K., Gao & Srivitsan, T., Modeling of void growth in ductile solids: effects of stress triaxiality and initial porosity. *Engineering Fracture Mechanics*, **71**, pp. 379–400, 2004.
- [5] Iturrioz, I., Morquio, A., Bittencourt, E. & d'Avila, V.R., Performance of the discrete element method to represent the scale effect. *Mecsol 2007*, 2007.
- [6] Sevostionov, I., Agnihotri, G. & Garay, J., On connections between 3-d microstructures and their 2-d images. *International Journal of Fracture*, **126**, pp. 65–72, 2004.
- [7] Terada, K. & Kikuchi, N., Nonlinear homogenization method for practical applications. *Computational Methods in Micromechanics*, **AMD-Vol. 212/MD-Vol. 62**, pp. ASME – 1–16, 1995.
- [8] Hill, R., (ed.), *The Elastic Behavior of a Crystalline Aggregate*, volume A-65, Phys. Soc., 1952.
- [9] Tvergaard, V. & Needleman, A., Analysis of the cup-cone fracture in a round tensile bar. *Acta Metallurgica*, **32**, pp. 157–169, 1984.
- [10] Goods, S. & Brown, L., The nucleation of cavities by plastic deformation. *Acta Metallurgica*, **27(1)**, pp. 1–159, 1979.
- [11] Dong, M., Prioul, C. & François, D., Damage effect on the fracture toughness of nodular cast iron: Part

i. damage characterization and plastic flow stress modelling. *Metalurgical and Materials Transaction A*, **28<sup>a</sup>**, pp. 2245–2254, 1997.

